Graphene-based fast electronics and optoelectronics

Ph. Avouris*, Y-.M. Lin, F. Xia, D.B. Farmer, Y. Wu, T. Mueller, K. Jenkins, C. Dimitrakopoulos, A. Grill
IBM T.J. Watson Research Center, Yorktown Heights, NY 10598
*avouris@us.ibm.com

Abstract: We present experimental results on high frequency field-effect transistors and fast photodetectors utilizing wafer-scale graphene grown epitaxially from silicon carbide.

Introduction

Graphene is a 2D electron system comprised of a single layer of carbon atoms arranged in a hexagonal honeycomb lattice. It is a zero-gap semiconductor with linear dispersion, vanishing rest mass, large carrier mobilities (200,000 $cm^2V^{-1}s^{-1}$ has been reported for suspended graphene [1]), strong and nearly constant optical absorption over a wide wavelength range (far IR to near UV), and excellent thermal and mechanical properties [2,3]. These characteristics make graphene ideally suited for fast analogue electronics and optoelectronics. Here, we demonstrate and discuss applications of graphene in radio-frequency (RF) transistors (>100GHz) and fast photodetectors (>50GHz). We also demonstrate the opening of a field-tunable electronic band gap in bilayer graphene.

RF graphene transistors

While the first experimental studies of electronic transport in graphene were performed on samples of mechanically exfoliated graphite [4], technological applications require large (wafer) scale, well characterized graphene. In our work we employ a technique based on the thermal decomposition of 4H(0001) SiC wafers at T • 1450°C to form a graphene-terminated wafer surface [5]. In order to fabricate RF transistors, this continuous graphene layer is patterned by oxygen plasma etching to electrically isolate the channel region, and source/drain electrodes are deposited by thermal metal (Pd/Au) evaporation. Top-gate stacks are then formed by either depositing an organic seed layer (NFC polymer) followed by HfO_2 or Al_2O_3 atomic layer deposition (ALD) [6] or by plasma enhanced chemical vapor deposition (PECVD) of a thin silicon nitride film [7], followed by gate metal deposition. Figures 1A and 1B respectively show a 2” wafer with arrays of RF graphene field-effect transistors (GFETs) fabricated using e-beam lithography and an individual GFET utilizing the NFC(10nm)/HfO_2(10nm) gate stack [8]. The RF performance of GFETs, such as those in Fig.1, is determined by measuring their S-parameters. Fig. 1C shows the frequency (f) dependence of the current gain (h21) for two such GFETs with a modest hole mobility of ~1,500 $cm^2V^{-1}s^{-1}$ and gate lengths of 550 nm and 240 nm [8]. After de-embedding, the current gain shows the expected 1/f dependence, and cut-off frequencies (f_T) of 53 and 100 GHz are respectively achieved. These are already excellent values

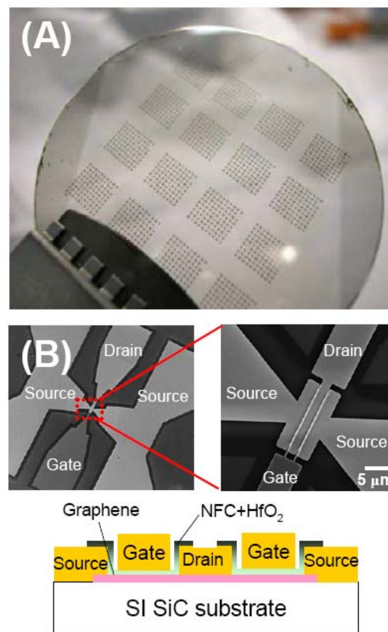

Figure 1. **(A)** Graphene wafer with an array of graphene RF transistors. **(B)** Images and schematic cross section of an individual transistor

given the early stage of development of this field and the long gate lengths used. We note that for a 240nm gate length Si-CMOS transistors are expected to give a f_T of 40 GHz.

The next steps in our efforts to improve device performance involve gate length scaling, decreasing the influence of access and contact resistances, and an improvement of the quality of the graphene material. In Fig. 2 we show the characteristics of another device with an effective gate length of ~ 90 nm and a source/drain separation of 160 nm. After de-embedding, the device exhibits cut-off frequencies of 130 GHz and 170 GHz at V_d = 1.7 V and 2.2 V, respectively. In this case, the RF performance of the device is limited by the access resistance associated with the ungated graphene regions, which are comparable in length to the gated channel region. We estimate that the RF performance and the cut-off frequency can be enhanced by a factor of two (~320GHz) for this 90-nm device by adopting a self-aligned structure that minimizes the access resistance. We recently developed a self-aligned gate fabrication process, which is based on the inherent nucleation inhibition of ALD gate insulator films on graphene [9]. The process currently produces access lengths of only 10-15 nm. Some initial results are shown in Fig.3. In other studies we have also demonstrated that the contact resistance itself can be reduced

from typically 0.5-2 kΩ·µm to about 200 Ω·µm for both contacts [10].

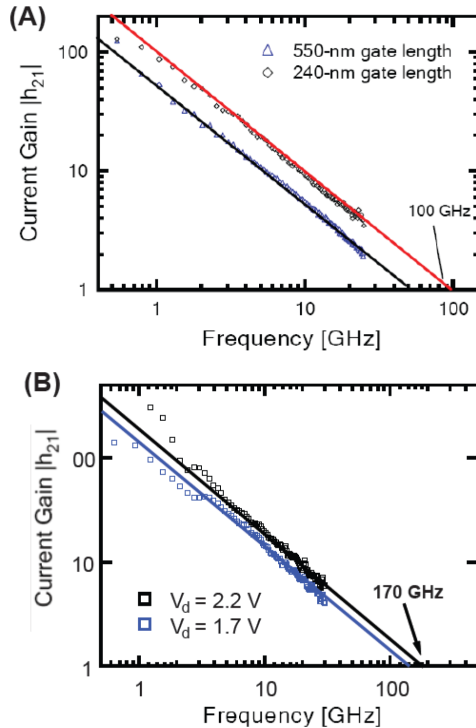

Figure 2. (A) Current gain (h_{21}) versus frequency plot of two RF transistors with gate lengths of 550nm and 240nm showing cutoff frequencies (f_T) of 53GHz and 100GHz, respectively [8]. (B) The characteristics of a 90nm gate length, 160 nm source-drain separation transistor. The f_T is 170 GHz.

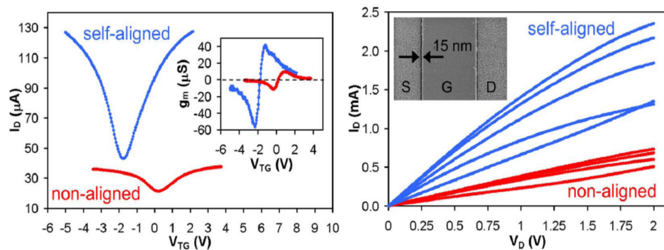

Figure 3. Comparison of a self-aligned device (blue) to a not self-aligned device with a 1 µm access length (red). **(A)** Transfer characteristics reveal a dramatic improvement in I_{ON}/I_{OFF} and transconductance (inset) when self-alignment is employed (V_D = 100 mV). **(B)** The output characteristics of the self-aligned device are also superior. Here, V_{TG} is swept from -4 V to 4 V in 2 V steps. A top-view SEM of a self-aligned device reveals that the separation of the source/drain and gate electrodes is approximately 15 nm (inset) [9].

In addition, the electrical quality of our epitaxial graphene has been improving. In Fig. 4 we give the mobility of Si-face SiC-derived graphene as a function of top-gate bias. [Christos] Hole mobilities twice as high as those used to produce the devices shown in Figs. 1 & 2 are obtained.

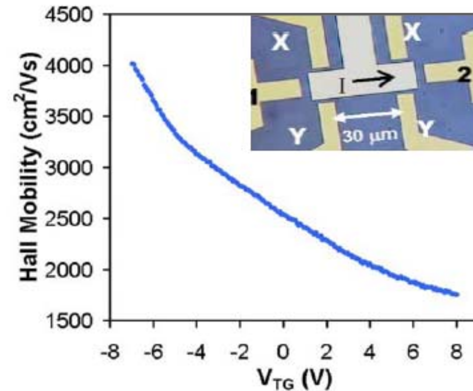

Figure 4. Top-gate bias dependence of the Hall effect mobility of epitaxially grown graphene from the Si-face of SiC [5]. Inset graphene Hall bar.

Opening a gap in bilayer graphene

Besides using graphene for analogue devices, there is a strong interest in opening a bandgap in graphene for optoelectronic applications and possibly even for digital electronics. One way to create a bandgap involves the application of a strong perpendicular electric field to AB-stacked, bi-layer graphene [11]. These bilayers have a four atom unit cell, hyperbolic dispersion, and no intrinsic bandgap. The low energy bilayer bandstructure involves two valence and two conduction bands. The field produces an asymmetry by inducing charge transfer between the layers. The two atoms in the bilayer unit cell that lie directly over each other are rather strongly coupled (~0.4eV) so the resulting charge-transfer breaks the inversion symmetry and opens a band-gap. A schematic illustrating the field-induced bandstructure changes is shown in Figure 5A. The upper valence and lower conduction bands move apart to form a direct bandgap slightly offset from the K-point. Optical absorption experiments have shown the feasibility of this scheme. [12,13] We have used dual-gated (top and bottom gates) GFETs with the NFC/HfO_2 gate stack (Fig. 5B) to open field-tunable bandgaps of more than 130 meV, and on/off ratios of ~100 at room temperature and >1000 at low temperatures.[14] Although this small gap is still not sufficient for digital applications, it could be utilized in optoelectronic applications such as THz emitters and detectors. Improvements in both the graphene and dielectric quality would allow further increases in the bandgap; a bandgap of ~ 400 meV has been predicted to be possible [3].

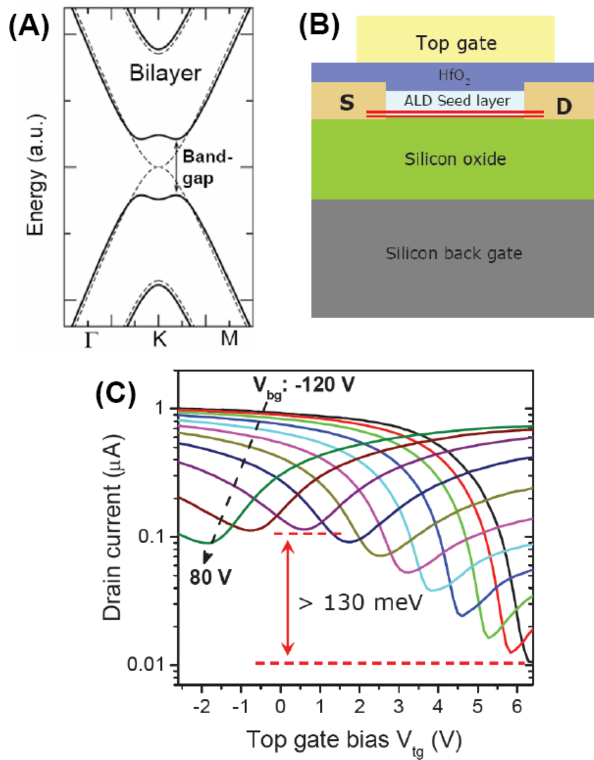

Figure 5. **(A)** Schematic illustration of band-gap opening in bi-layer graphene by a perpendicular electric field. Dashed line denotes the potential with no applied field, while the solid line the potential with a high applied field. **(B)** Schematic of the structure of the device used to open the gap. **(C)** Room temperature transfer characteristics of a double-gated bi-layer graphene FET. The back-gate bias, V_{bg}, is varied from -120 to 80V at steps of 20V [14].

Fast graphene photodetectors

The light trasmittance (T) of free-standing graphene can be shown theoretically to be: $T = (1+\pi\alpha/2)^{-2} \approx 1-\pi\alpha \approx 0.977$, [15] where α is the fine structure constant $\alpha \approx 1/137$. Thus, single-layer graphene should transmit ~ 97% of the incident light and absorb ~ 2.3%, independent of the wavelength of the light [15]. Indeed, a number of experimental studies have verified the ~ 2.3% inter-band absorption in graphene monolayers over a wide wavelength scale spanning the visible and infrared ranges. Moreover, the absorbance of multilayers at energies above ~0.5eV is additive [15]. The wide range and constant absorption of graphene make it a desirable material for photodetectors. In addition, the fast carrier transport and the fact that, unlike in conventional semiconductors, both components of the photo-excited e-h pair have high mobilities suggest a very fast response of such a detector. However, graphene is a zero gap semiconductor. If a voltage is applied across it, a large dark current develops, which leads to large shot-noise. For this reason, we focused on the properties of graphene-metal contacts. In contacts that preserve the structural integrity of graphene under the metal, such as Pd-graphene contacts, there is charge-transfer between the two systems and the graphene becomes doped. This leads to a 'band-bending' that extends to a depth of the order of 100 nm into the graphene channel. [16,17] As a result, a built-in electric field is generated near the contact. Photoexcitation near a contact generates e-h pairs that can be separated by the built-in field to produce a net photocurrent. [16,17]. A schematic illustration of these effects is shown in Fig. 6. The field direction at the source and drain contacts should be opposite. Therefore, in a symmetric device, simultaneous illumination of both contacts leads to equal but opposite polarity currents and no net photocurrent. Indeed, our near field photocurrent imaging studies verify that photoexcitation near contacts leads to zero-bias photocurrent of opposite polarity at the two contacts as shown in Fig. 7 [17].

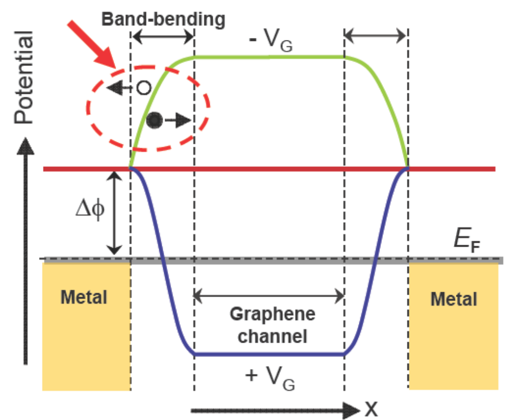

Figure 6. Schematic potential energy diagram of the bending of the graphene bands near the metal contacts and the separation of photo-excited electron-hole pairs.

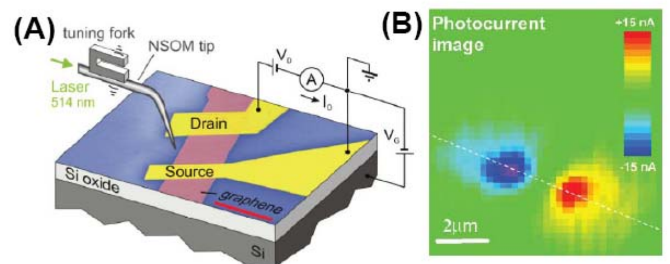

Figure 7. **(A)** Illustation of the device and set up used for zero-bias photocurrent imaging of graphene. **(B)** Photocurrent image of the contacted graphene. Photocurrent is generated near the two metal-garpahene contacts and has opposite polarity at source and drain [17].

Figure 8 shows the frequency dependence of the photoresponse of a graphene photodetector for illumination of

one contact at 1.55 µm [18]. No degradation in the photoresponse was observed up to the frequency limit of the measurement system (40 GHz), and simple estimates indicate that the maximum frequency should be limited by the RC constant of the devices to about ~ 0.5 THz [18].

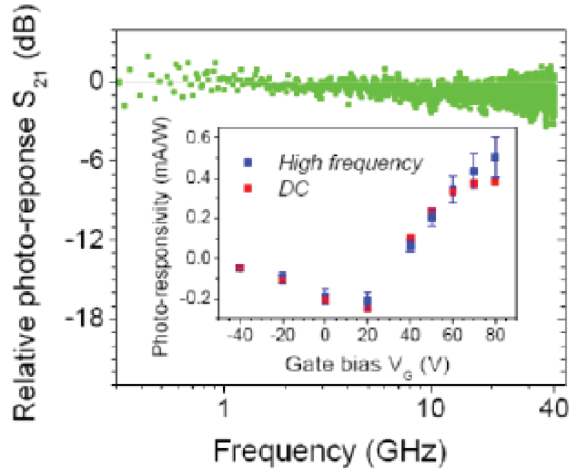

Figure 8. Relative photoresponse (S_{21}) of a two-electrode graphene photodetector as a function of the modulation frequency of the 1550 nm light illuminating one contact. Inset: Comparison of the RF and DC photoresponses of this device.

Improvements to the simple photodetector described above involve generating a device that utilizes the full surface of graphene for photodetection and an increased value of the photoresponse. Such a structure is shown in Fig. 9 [19]. It involves multiple interdigitated electrodes made of two different metals. One with a high, in this case Pd, and one with a low, in this case Ti, workfunctions. At appropriate back-gate biases, the two different workfunctions and resulting asymmetric band-bendings generate a sloping overall potential along the graphene channel that allows photodetection over the entire device [19]. Furthermore, the multi-finger electrodes allow larger photocurrents to be generated. This type of device was tested and found to be able to reliably detect optical data streams of 1.55 µm light pusles at a rate of 10 GBits/s (maximum capability of the measurement system) without an applied source-drain bias [19]. Error-free detection at 10 GBits/s was verified by the open eye measurement shown in the bottom of Fig. 9.

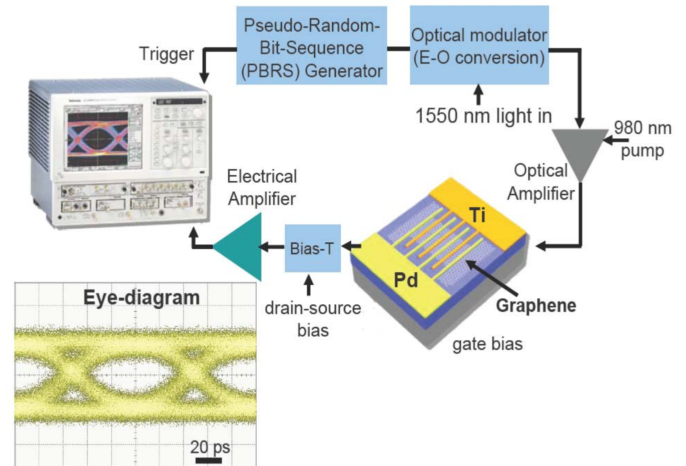

Figure 9. Schematic and SEM of the multi-finger, two-different metal graphene photodetector and its utilization to detect optical data streams at 19Gbit/s. Bottom: Open eye test indicating error-free detection of optical data at 10GBits/s [19].

Acknowledgements

We would like to thank Chun-Yung Sung for his support and encouragement of this work and Bruce Ek for his expert technical support. Financial support was provided by DARPA under contract FA8650-08-C-7838 (CERA program).

References

[1] K. I. Bolotin et al. *Solid State Commun*. 146, 351 (2008)
[2] A. K. Geim, K.S. Novoselov, *Nat. Mater*. 6, 183, (2007)
[3] A.H. Castro Neto et al. *Rev. Mod. Phys*. 81, 109 (2009)
[4] K.S. Novoselov et al. *Science* 36, 666 (2004)
[5] C. Dimitrakopoulos et al. *J. Vac. Sci. Technol.* B 28, 985 (2010).
[6] D.B. Farmer et al. *Nano Lett.* 9, 4474 (2009)
[7] W. Zhu et al. *Nano Lett*. (2010), DOI: 10.1021/nl101832y
[8] Y.-M. Lin et al. *Science* 327, 662 (2010)
[9] D.B. Farmer et al. *Appl. Phys. Lett*. 97, 013103 (2010)
[10] F. Xia et al., submitted for publication.
[11] E. McCann, *Phys. Rev. B* 74, 161403(R) (2006)
[12] F. Wang et al. *Science* 320, 206 (2008)
[13] K.F. Mak et al. *Phys. Rev. Lett*. 101, 196405 (2008)
[14] F. Xia et al. *Nano Lett.* 10, 715 (2010)
[15] R.R. Nair et al. *Science* 320, 1308 (2008)
[16] F. Xia et al. *Nano Lett.* 9, 1039 (2009)
[17] T. Mueller et al. *Phys. Rev*. B 79, 245230 (2009)
[18] F. Xia et al. *Nature Nano* 4, 839 (2009)
[19] T. Mueller et al.*Nature Photon*. 4, 29 (2009)